*Type of the Paper (Article)*

# Complex Mutation Pattern of Omicron BA.2: Evading Antibodies without Losing Receptor Interactions

**Saathvik R. Kannan[1,¶], Austin N. Spratt[1,¶], Kalicharan Sharma[2,¶], Anders Sönnerborg[3], Subbu Apparsundaram[2], Christian L. Lorson[1,3], Siddappa N. Byrareddy[4,5,6,*] and Kamal Singh[1,2,3,7,*]**

[1] Bond Life Sciences Center, University of Missouri, Columbia, Missouri, USA. skannan@missouri.edu; ans3mm@missouri.edu

[2] Department of Pharmacology, Delhi Pharmaceutical Sciences and Research University, New Delhi, India. sharmakcpt@gmail.com ; Subbu.apparsundaram@gmail.com

[3] Department of Veterinary Pathobiology, University of Missouri, Columbia, Missouri, USA. lorsonc@missouri.edu; singhka@missouri.edu

[4] Department of Pharmacology and Experimental Neuroscience, University of Nebraska Medical Center, Omaha, Nebraska, USA. sid.byrareddy@unmc.edu

[5] Department of Genetics, Cell Biology and Anatomy, University of Nebraska Medical Center, Omaha, Nebraska, USA. sid.byrareddy@unmc.edu

[6] Department of Biochemistry and Molecular Biology, University of Nebraska Medical Center, Omaha, Nebraska, USA. sid.byrareddy@unmc.edu

[7] Division of Clinical Microbiology, Department of Laboratory Medicine, Karolinska Institute, Stockholm, Sweden. anders.sonnerborg@ki.se; kamlendra.singh@li.se

¶These authors contributed equally.

* Correspondence: Siddappa N. Byrareddy (sid.byrareddy@unmc.edu)
Kamal Singh (singhka@missouri.edu); kamlendra.singh@ki.se

**Abstract:** BA.2, a sublineage of Omicron BA.1, is now prominent in many parts of the world. Early reports indicate that BA.2 is more infectious than BA.1. To gain insight into BA.2 mutation profile and the resulting impact of mutations on interaction with receptor and/or monoclonal antibodies, we analyzed available sequences, structures of Spike/receptor, and Spike/antibody complexes, and conducted molecular dynamics simulations. The results showed that BA.2 has 50 high-prevalent mutations compared to 48 in BA.1. Seventeen BA.1 mutations are not present in BA.2. Instead, BA.2 has 19 unique mutations and a signature Delta variant mutation (G142D). Intriguingly, the BA.2 has 28 signature mutations in Spike, compared to 30 in BA.1. This is due to two revertant mutations S446G and S496G in the receptor-binding domain (RBD), making BA.2 somewhat similar to Wuhan-Hu-1 (WT), which has G446 and G496. The molecular dynamics simulations showed that the RBD consisting of G446/G496 is more stable than S446/S496 containing RBD. Thus, our analyses suggest that BA.2 has evolved with novel mutations (i) to maintain receptor binding similar to WT, (ii) evade the antibody binding greater than BA.1, and (iii) acquire mutation of the Delta variant that may be associated with the high infectivity.

**Keywords:** COVID-19; SARS-CoV-2; Viruses; Omicron BA.1, BA.2, Delta.

## 1. Introduction

Severe Acute Respiratory Syndrome coronavirus 2 (SARS-CoV-2), the causative agent of Coronavirus Disease 2019 (COVID-19) has been evolving in the form of variants since its emergence in 2019 [1]. Several variants containing different mutation clusters have emerged when compared to the ancestral Wuhan-Hu-1 strain [2-5]. Based upon a number of infection-related criteria, including transmissibility, disease severity, decrease in neutralization, responsiveness to therapeutics, and detection sensitivity, the variants have been classified as a variant of concern (VOC), variant of interest (VOI), or variant

Preprints (www.preprints.org) | NOT PEER-REVIEWED | Posted: 13 April 2022 doi:10.20944/preprints202204.0120.v1

being monitored (VBM). To date, five VOCs: Alpha (B.1.1.7), Beta (B.1.351), Gamma (P.1), Delta (B.1.617.2) and Omicron (B.1.1.529) have been identified.

The most recently identified variant is Omicron, which includes lineage B.1.1.529 and sublineages BA.1, BA.1.1, BA.2 and BA.3 as classified by the World Health Organization (https://www.who.int/en/activities/tracking-SARS-CoV-2-variants) [6,7]. To gain insight into BA.2 mutation profile, we analyzed available sequences (n = 8660) (as of Feb. 2022) for the prevalence of BA.2 signature mutations. We also analyzed available structures of Spike receptor binding domain (S-RBD) of Wuhan-Hu-1 or Omicron strains in complex with monoclonal antibodies (mAbs) to understand the function of mutations at the interface. Our analyses showed a significant difference in the number and distribution of mutations between BA.2 and Omicron BA.1. The structural data show that BA.2 has evolved such that it maintained critical contacts with ACE2 that are essential for viral entry yet has the capability to escape (or reduce) the binding of mAbs. A combination of these two factors renders BA.2 an alarming variant that may impact current and future vaccination strategies.

## 2. Results

### *2.1. Prevalence of BA.2 signature mutations*

High-quality, high-coverage sequences (n=8,660) from GSAID [8] were used to identify the distribution of mutations in BA.2. Since BA.2 is not classified as a variant in the GSAID repository, we used a combined search criterion (VOC Omicron GRA plus Spike_T376A) to filter the sequences corresponding to BA.2. In addition, we used NextClade [9], and an in-house Python script to process sequences for the identification of the BA.2 signature mutations. Overall, we identified a total of 50 signature mutations in the BA.2 variant (with ~100% prevalence), compared to 48 mutations present in Omicron BA.1 [10] (**Tables 1 and 2**). Additionally, 17 mutations of BA.1 are not present in BA.2, and BA.2 has 19 novel mutations that are not signature mutations of BA.1.

More than half (56%) of all BA.2 signature mutations (28 out of 51) are present in the S-protein (**Table 1 and 2**). In contrast, 75% of all mutations in BA.1 are present in the S-protein BA.1 [10] (**Table 1**). These signature BA.2 mutations within S-protein are ~100% correlated (i.e., 100% coexisting). Eight of 28 mutations (T19I, PPA25-27Del, G142D, V231G, S371F, T376A, D405N, and R408S) are unique to BA.2 (i.e., these mutations are not present in BA.1), and 12 of 32 mutations (A67V, T95I, VYY143-145Del, N211Del, S212I, R214EPEins, S371L, G446S, G496S, T547K, N856K and L981F) within the BA.1 S-protein are not present in BA.2. There are 20 common mutations between BA.1 and BA.2. Mutation at position 371 is present in both BA.2 and BA.1. However, BA.2 has S371F whereas BA.1 has S371L mutation. It is interesting to note that a majority of mutations (24 out of 28) in BA.2 S-protein are in the S1 subunit, which participates in the initial binding of the receptor, and is cleaved during virus entry. A notable mutation in BA.2 is G142D, which is also a signature mutation in the Delta variant [3].

### *2.2. Analysis of structural data and impact of mutations on overall S-RBD structure*

As of February 25, 2020, 571 S-protein related structures have been deposited to the Protein Data Bank (PDB) [11]. Of these, 88 have been solved by the X-ray crystallography, whereas 483, by Cryo-Electron Microscopy (Cryo-EM). These structures include S-protein in apo form (*i.e.,* alone), S-protein (or S-RBD) in complex with ACE2, and S-protein (or S-RBD) bound to antibodies/nanobodies. These structures also include 23 Omicron variant S-protein structures either in apo form or in complex with ACE2 or in complex with an antibody. Twenty-two of these structures have been solved by Cryo-EM with resolution ranging between 2.45 Å and 3.88 Å, whereas one structure was solved by the X-ray crystallography (PDB entry 7TN0) [12]. Comparative analyses of the S-protein apo structure with S-protein (or S-RBD) in complex with ACE2 and/or antibody provide insights into the structural changes adopted by S-protein to bind the co-factors.

Preprints (www.preprints.org) | NOT PEER-REVIEWED | Posted: 13 April 2022 doi:10.20944/preprints202204.0120.v1

**Table 1.** Unique mutations in BA.1 and BA.2 within the S-protein

| BA.1 (Original)* | BA.2* |
|---|---|
| | T19I |
| | PPA25-27Del |
| A67V | |
| T95I | |
| | G142D |
| VYY143-145Del | |
| N211Del | |
| L212I | |
| | V213G |
| R214EPEins | |
| S371L | S371F |
| | T376A |
| | D405N |
| | R408S |
| G446S | |
| G496S | |
| T547K | |
| N856K | |
| L981F | |

To assess if variant-specific mutations impart any structural changes in the overall structure of S-RBD, we superposed S-RBD from Wuhan-Hu-1 S-RBD/ACE2 complex (PDB entry 6M0J) [13] on the S-RBD from Omicron BA.1 S-protein/ACE2 complex (PDB entry 7T9K) [14]. The two S-RBD superposed extremely well with a root mean square deviation (RMSD) less than 0.5 Å between 196 C$\alpha$ atoms of the S-RBDs. This comparison suggests that despite a large number of mutations (16 in total) in Omicron BA.1 S-RBD, the overall structure of S-RBD remains unchanged. The PDB entry 7TN0 [12] contains Omicron BA.1 S-RBD bound to a broadly neutralizing sarbecovirus monoclonal antibody (mAb) S309 (the parent mAb of sotrovimab) and human ACE2. To assess if the mutations in BA.1 caused the structural changes, in Omicron BA.1 S-RBD upon binding to both ACE2 and mAb, we superposed the S-RBD structure from PDB file 7TN0 (Omicron S-RBD) onto S-RBD of Wuhan-Hu-1 (PDB entry 6M0J) [13]. The S-RBDs from these strains superposed exceptionally well with less than 0.5 Å RMSD between 196 C$\alpha$ atoms, suggesting that no significant change in the overall structure of S-RBD occure upon binding to mAb or ACE2. This structural analysis suggests that neither variant-specific mutations nor binding to mAbs causes any significant change in the structure of S-protein. Hence, the impact of mutations on the binding of mAbs is likely through the local structural changes such as readjustment of sidechains or loop conformations that may affect direct polar/nonpolar interactions between S-protein and mAbs.

*2.3. Impact of mutations on S-RBD/ACE2 interaction*

The structure of Omicron BA.1 bound to ACE2 (PDB entry 7T9K) [14] shows that seven BA.1 signature mutations (G446S, T478K, E484A, Q493R, G496S, Q498R and N501Y) are within interacting distance of ACE2 [10]. Additionally, K417 and Y505 interact with ACE2 residues (PDB entry 6M0J [13], which represents a WT S-RBD (Wuhan-Hu-1). However, interactions of K417 and Y505 are lost when BA.1 acquired K417N and Y505H mutations. Two recent reports showed that Omicron BA.1 S-RBD binds with greater affinity with ACE2 than WT S-RBD [14-15]. We used the PDBePISA server [16] to determine the interactions between BA.1 S-RBD and ACE2 and WT S-RBD and ACE2 using PDB entries 7T9K and 6M0J, respectively. No significant difference in the buried surface area was noted but there are two additional interactions in BA.1: a salt-bridge between R498 (as a result of Q498R in BA.1) and a hydrogen bond between S496 of BA.1 S-RBD and K353 of

Preprints (www.preprints.org) | NOT PEER-REVIEWED | Posted: 13 April 2022 doi:10.20944/preprints202204.0120.v1

ACE2. These additional interact may partly suffice for a marginally better binding of BA.1 S-RBD to ACE2 compared to that of WT S-RBD to ACE2.

*2.4. BA2 unique mutations in relation to mAb binding*

Mutation K417N is retained in BA.1 but S496 is reverted to G496 (as in the WT). In fact, there are two mutations in BA.2, which have been reverted to the WT residues, *i.e.*, to G446 and G496. In the crystal structure of WT S-RBD/ACE2 complex (PDB entry 6M0J), G446 and G496 participate in a network of interactions through their backbone that also involve Q42, D38 and K353 from ACE2 and G446, Y449 and G496 from S-RBD (**Fig. 1A**). These interactions are expected to remain unchanged with G446S and G496S mutations (as in BA.1) as they are through the peptide backbone. However, there are two additional signature mutations in the vicinity of 446 and 496: Q498R, and N501Y. The larger sidechains of R498 and Y501 require adjustments in local structure that is achieved by the change in loop conformation housing G446/S446 (**Fig. 1B**). A similar conformational change in the loop housing G496/S496 is significantly less evident (**Fig. 1B**). An adjustment in loop conformation renders the loss of S446/S496 backbone interactions with ACE2 as the backbone atoms of S446 and S496 are not within the interacting distance of ACE2 residues (shown in red dotted line) (**Fig. 1C**). However, new interactions between BA.1 S-RBD and ACE2 are generated, which compensate the loss of interactions through the backbone of S446 and S496. Conformational adjustments in this region may also be due to the property of glycine residue or other mutations in this region in different VOCs including Q498R (BA.1 and BA.2), G496S (BA.1), N501Y (Alpha, Beta, Gamma, BA.1 and BA.2), and Y505H (BA.1 and BA.2) (**Fig. 1D**). Hence, it appears that the BA.2 variant not only retained the interactions of BA.1 with ACE2 but also reacquired the interactions seen in the Wuhan-Hu-1.

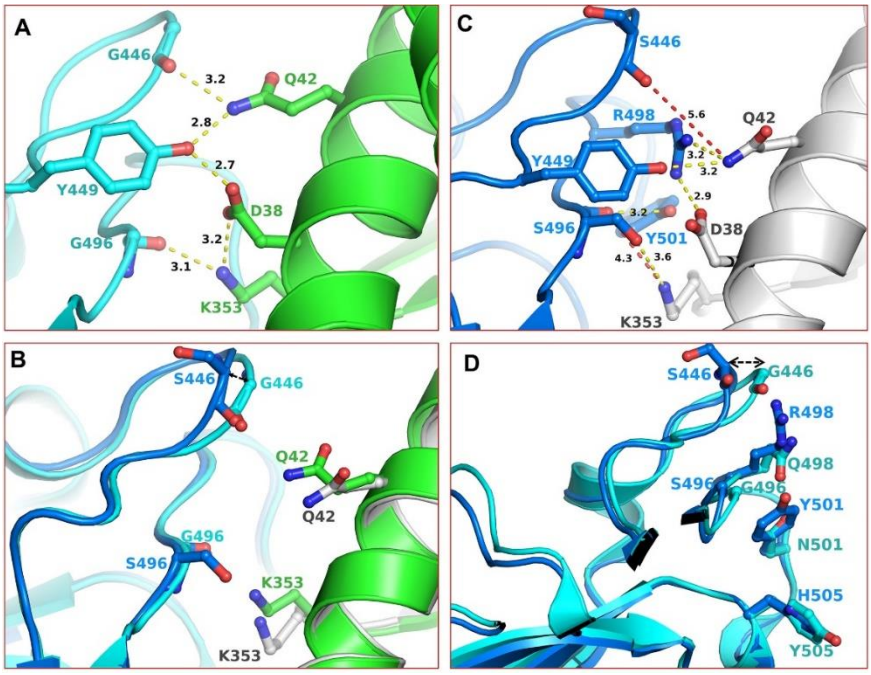


**Figure 1. Interactions between S-RBD and ACE2 and impact of mutations. Panel A** shows the interaction network between S-RBD and ACE2 created by G446 and G449 (as in BA.2), the two residue positions that were reverted to WT sequence in BA.2 when compared to BA.1, which has S446 and S496, respectively. This figure was generated from PDB entry 6M0J [13]. The amino acid residues are shown in ball-and-sticks representation. The S-RBD is in cyan color and ACE2, in green. The carbon atoms are colored in same color as in the molecule (S-RBD or ACE2). In this and in subsequent panels and figures, the oxygen atoms and red, nitrogen atoms, blue. All distances in this and in subsequent figures ate in Å. **Panel B** shows the conformational change in the loops containing G/S446 and G/S496. WT-like S-RBD is colored in cyan and BA.1 S-RBD, in teal. ACE2 of WT S-RBD

Preprints (www.preprints.org) | NOT PEER-REVIEWED | Posted: 13 April 2022 doi:10.20944/preprints202204.0120.v1

is green and that of BA.1 is gray. **Panel C** shows that mutation G446S and G496S (as in BA.1). These mutations cause conformational change of the loop that comprises of 446 and 496 positions. This figure was generated from PDB entry 7T9K, which represents the structure of BA.1 S-RBD/ACE2 complex [14]. **Panel D** shows common mutations (except S446 in BA.1 and G446 in BA.2) lined at the interaction surface of S-RBD and ACE2. The color code for molecules is same as that in **Panel C**.

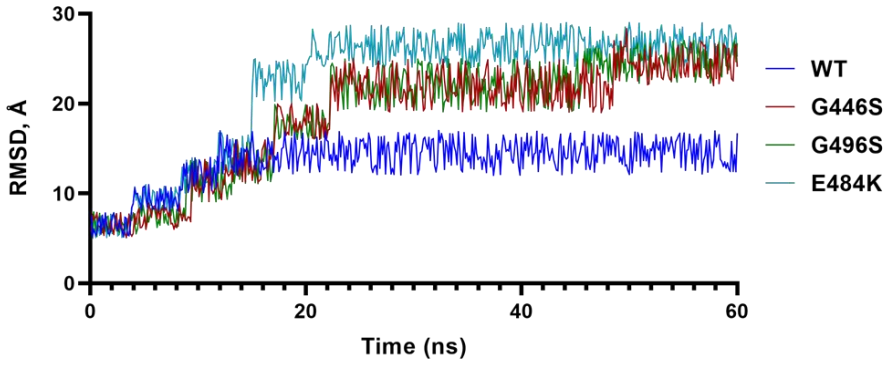


**Figure 2. Molecular Dynamics simulation.** Trajectory of the root-mean square deviation of S-RBD C$\alpha$-atoms of E484A, G446S/G496S and G446/G496 over 100 ns MD simulations.

To further understand the impact of G residues at 446 and 496 as in the WT and BA.2, we conducted molecular dynamics (MD) simulations of G and S containing S-RBDs, and included the E484A mutation as a comparison (**Fig. 2**). The results show that the G446/G496 combination stabilizes at 15 ns whereas S446/S496 takes longer (~23 ns) to stabilize and the RMSD of S446/S496 remains greater than G446/G496. These data suggest that the S-RBD containing G446/G496 is more stable than S446/S496, and that greater stability of G446/G496 may be one of many advantages for BA.2 to evolve with reverted WT-like residues.

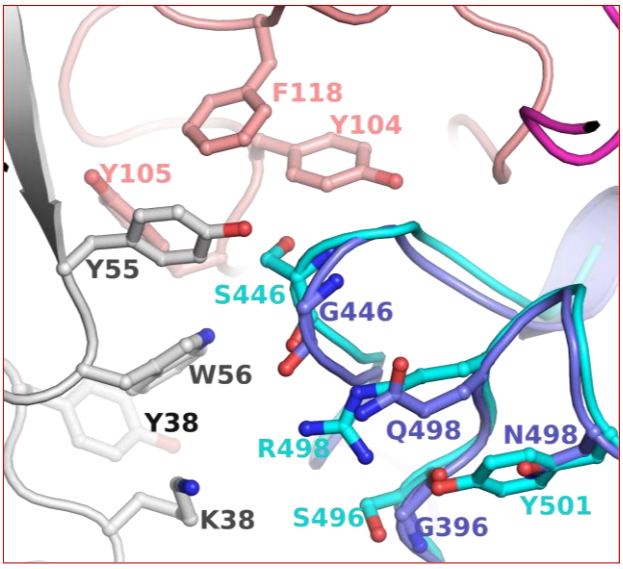


**Figure 3. Position of G446/G449 in relation to mAb.** This figure shown mAb (AZD1061) bound WT S-RBD (PDB file 7L7E). To assess the change in loop conformation housing G446 and S446, we superposed the S-RBD of BA.1 bound to S304/309 mAbs (PDB entry 7TN0). The WT S-RBD is rendered in purple ribbons whereas BA.1, in cyan ribbons. The heavy and light chains of AZD1061 are rendered in deep salmon and grey, respectively. The carbon atoms are colored is same color as the ribbons. The other atoms are colored as defined in **Fig. 1**.

To explore the possibility if revertant mutations S446G and S496G evolved to evade mAb binding, we examined available structures of S-protein (or S-RBD) bound to

Preprints (www.preprints.org) | NOT PEER-REVIEWED | Posted: 13 April 2022 doi:10.20944/preprints202204.0120.v1

antibodies. A crystal structure of WT S-RBD in complex with human monoclonal antibodies AZD8895 (tixagevimab) and AZD1061 (cilgavimab) has been reported (PDB entry 7L7E) [17]. The combination of the two mAbs has been considered as long-acting regimen developed by AstraZeneca and Vanderbilt [18]. The mAb bound S-RBD structure in shown in **Fig. 3.** To assess the change in loop conformation housing G446 and S446, we superimposed the S-RBD of BA.1 bound to S304/309 mAbs (PDB entry 7TN0) [12]. This model clearly demonstrates that G446 and 496 are the part of the mAb binding region which contains a cluster of hydrophobic residues. it is possible that the revertant mutations (S446G and S496G), in combinations with other BA.2 in this region, evolved to escape the binding of AZD8895, AZD1061, S304 and/or S309.

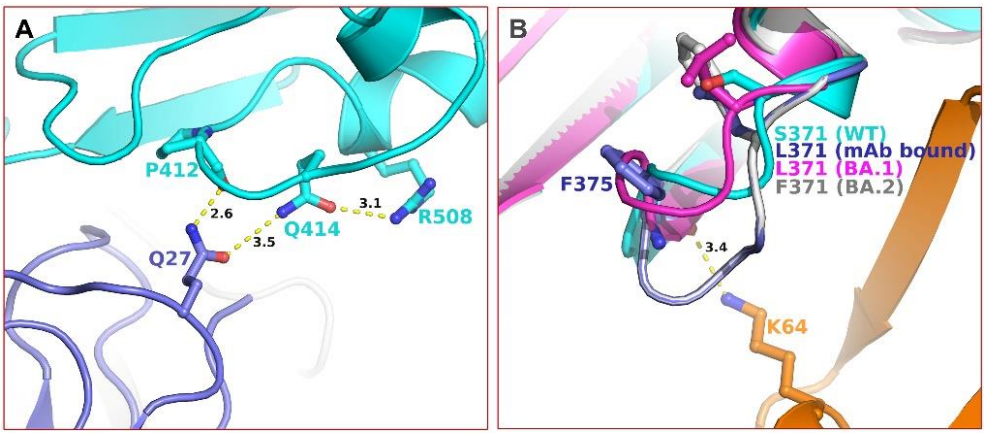


**Figure 4. Position of unique BA.2 mutations at the interface of mAb S409 and S403 and S-RBDs.** Panel A shows the interaction network of R408 with S403 mAb light chain (purple) and S-RBD (BA.1) (cyan). A unique mutation of BA.2 (R408S) is expected to disrupt this interaction pattern and thereby, the binding affinity of the mAb with S-RBD. Panel B shows the change in the conformation of loop containing S371 (WT, cyan), L371 (BA.1, magenta) (PDB entry 7T9K), BA.1 bound to S304 mAb (purple) (PDB file 7T90) and modeled S371F BA.2 mutation (grey). The interactions between mAb S409 heavy chain orange) and S-RBD (BA.1) is shown in dotted line.

Four other mutations in BA.2 S-RBD (S371F, T376A, D405N, and R408S) differ from BA.1 (**Table 1**). Analyses of BA.1 S-RBD/S304/S309 crystal structure complex also provides some insights into the evolution of BA.2 to escape (or reduce) binding with these two mAbs. In BA.1 S-RBD bound S304 crystal structure, R408 forms a hydrogen bond with Q414 which, in turn, forms a hydrogen bond with Q27 of S304 light chain (**Fig. 4A**). Glutamine 27 of S309 also interacts with the mainchain C=O group of P412. A mutation R408S would most certainly disrupt this interaction network, leading to a reduced mAb binding to S-RBD if not completely abolish. Residue position 371 is part of the loop formed by residues 366 to 375, a region that is highly flexible as reported before [12]. Additionally, this region already contains two phenylalanine residues. A mutation S375F (as in BA.2) (**Fig. 4B**) adds another phenylalanine rendering an extremely hydrophobic region, which most likely will affect the loop conformation, and any conformational change in this loop region is bound to impact interactions between S-RBD and heavy chain of S304 mAb.

*2.5. BA2 unique mutations in relation N-terminal directed mAb binding*

The N-terminal domain of the BA.2 S1 subunit also has four unique mutations (Table 1). One of these mutation G142D is a signature mutation of highly infectious and pathogenic Delta variant [19]. We have previously shown how G142D mutation can evade mAbs [3]. Thus, BA.2 can evade mAb recognition through a similar mechanism as the Delta variant.

*2.6. BA2 unique mutations in ORFs other than the S-protein*

In addition to mutations in BA.2 S-protein, there are 22 high-prevalent mutations (~100%) throughout the rest of the BA.2 genome. Eleven of these 22 mutation are unique to BA.2 (*i.e.*, not present in BA.1). Whereas, only 5 out of 16 mutations are unique to BA.1

Preprints (www.preprints.org) | NOT PEER-REVIEWED | Posted: 13 April 2022 doi:10.20944/preprints202204.0120.v1

(Table 2). Additionally, there are 11 common mutations between BA.1 and BA.2. Unique mutations in BA.2 in different non-structural proteins (nsps) may have diverse roles such as altering the intra- and inter-nsp interactions. For example, mutation R391C in nsp14 (exoribonuclease) is close to the nsp12 (RNA dependent RNA polymerase) in the complex, representing a replication-transcription complex (RTC), which consists of nsp7, nsp8, nsp9, nsp10, nsp12, nsp13, and nsp14 (PDB entry 7EGQ) [20]. Hence, this mutation may impact the arrangement of the RTC.

**Table 2:** Unique BA.1 and BA.2 mutations in genes other than S-protein

| BA.1 (Original) | BA.2 |
|---|---|
| M:D3G | |
| | N:S413R |
| | nsp1:S135R |
| | nsp3:T24I |
| nsp3:K38R | |
| nsp3:L1266I | |
| | nsp3:G489S |
| nsp3:A1892T | |
| | nsp4:L264F |
| | nsp4:T327I |
| | nsp4:L438F |
| nsp6:I189V | |
| | nsp14:R391C |
| | nsp15:T112I |
| | ORF3a:T223I |
| | ORF6:D61L |

Similarly, a common (BA.2 and BA.1) nsp5 ($M^{pro}$) mutation P132H is located between two domains of nsp5 crystal structure bound to the Pfizer protease inhibitor PF-07321332 (PDB entry 7VH8) [21]. Mutation H132 can form a salt bridge with E240 from the adjacent domain and provide additional stabilization between two domains. Unfortunately, extrapolating the function of mutation in nsps is not as straightforward as with mutations S-protein mutations.

## 3. Discussion

SARS-CoV-2 has been evolving in the form of variants by mutations in Wuhan-Hu-1 that emerged more than two years ago. Most of these variants have been more infectious and pathogenic than the ancestral Wuhan-Hu-1 virus. As with all RNA viruses, the evolution of SARS-CoV-2 and the development of subsequent VOCs is not unique. However, for a virus that is equipped with proofreading machinery (nsp14), the rapid rate of viral evolution is surprising. Here, we presented the analyses of the mutations in BA.2 and compared with BA.1, the original Omicron variant. It appears that BA.2 has evolved to retain a majority of mutational profile of BA.1, but acquired additional mutations such as G142D of Delta variant to escape (or reduce) the binding with mAbs, and reverted at some position to WT residues (such as G446 and G496) as in) to maintain receptor binding properties of Wuhan-Hu-1. Additionally, the BA.2 variant evolved to harbor particularly relevant mutations that are present at the interface with S-protein and antibodies. The

 doi:10.20944/preprints202204.0120.v1

extrapolation of function for mutations in ORFs other than the S-protein encoding region is not straightforward for two reasons: (i) the number of reported S-protein structures is far more than other nsp structures, and (ii) it is difficult to structurally predict the impact of mutations in proteins that are largely enzymatic in function (such as nsp3, nsp5, nsp12 and nsp13) unless a highly conserved active site is mutated.

In summary, evolution of a virus like BA.2 appears extraordinary as BA.2 has seemingly evolved to encompass the "best" of the both worlds: reduced susceptibility to neutralizing antibodies, yet with receptor-mediated entry activity at least as good as the wild-type virus. The fortuitous mutation positions in BA.2 at the interface of S-protein and antibodies makes one wonder what factors have contributed to the rapid evolution of this virus. Potentially the virus has evolved under the pressure of previously existing antibodies either induced by the vaccination (as very recently reported [22]) or previous infections, or perhaps new lineages emerged from unvaccinated or immunocompromised individuals.

## 4. Materials and Methods

### *4.1. Sequence acquisition and analysis*

The prevalence of each mutation in BA.1 and BA.2 was obtained from the GISAID repository [8]. These sequences were aligned using the MAFFT [23], MEGA X [24] or JalView [25] sequence alignment programs to identify BA.2 signature mutations. These sequences were analyzed for amino acid changes using Nextclade and later processed using an in-house Python script to identify the prevalence of mutations in BA.2. Any mutation with greater than 50% prevalence was considered as a signature mutation.

### *4.3. Structural analysis*

An in-house R program was written to retrieve sequences from the Protein Data Bank (www.rcsb.org). Specific structures were extracted using the 'grepl' function of the R package 'dplyr'. The structures were then downloaded and analyzed using either the Schrodinger Suite (Schrodinger LLC, NY) or PyMol [26].

### *4.3. Molecular dynamics (MD) simulation*

The crystal structure of S-RBD bound ACE2 (PDB file 6M0J) [13] was used as WT SARS-CoV-2 S-RBD. All MD simulations used TIP3P [27] water filled truncated, isometric, octahedron periodic boxes containing solutes to a 12 Å depth. A minimum of 10 $Na^+$ and $Cl^-$ ions were used to neutralize the charge and to the increase ionic strength to 145 mM. Monovalent ion positions were randomized at 5.0 Å from other solute atoms and 3.0 Å from each other using different seeds to generate five distinct model replicates. The simulation was run at a temperature of 300 K with a pressure of 1.013 bar for a duration of 100 ns. Trajectories and trajectory files were analyzed and generated by VMD [28].

**Author Contributions:** KS (K Singh) conceptualized the study; KS (K Singh) wrote the first draft, and KS (K Singh), SNB, SA and CLL wrote the final manuscript. ANS, SRK, and KS (K Singh) conducted genetic analyses, wrote required programs either in R or in Python; KS (K Sharma) and KS (K Singh) conducted structural analysis of Spike/antibody complex; SNB, RKG, AS and CLL edited the manuscript and contributed to understanding the pathogenicity of CoVs. All authors approved the final manuscript.

**Funding:** Please add: This work was partially supported by National Institute of Allergy and Infectious Diseases grants R01 AI129745, R01 AI113883, and DA052845 to S.N.B. Further, S.N.B. acknowledges independent research and development (IRAD) funding from the National Strategic Research Institute (NSRI) at the University of Nebraska. K. Singh was partially funded by the Bond Life Sciences Center (Early Concept Grant) and University of Missouri startup support. SNB acknowledge the support by the National Institute of Allergy and Infectious Diseases (3R21AI144374-02S1).

**Acknowledgments:** KS (K Singh) acknowledges the computation facilities of the Molecular Interactions Core at the University of Missouri, Columbia, MO 65212. We thank the laboratories that have generously deposited sequences into the GISAID database.

 doi:10.20944/preprints202204.0120.v1

**Conflicts of Interest:** CLL is co-founder of Shift Pharmaceuticals, Overland Park, KS, USA. KS (K Singh) is consultant of Sanctum Therapeutics Corporation, Sunnyvale, CA, USA.

## References


1. Wu, F.; Zhao, S.; Yu, B.; Chen, Y.M.; Wang, W.; Song, Z.G.; Hu, Y.; Tao, Z.W.; Tian, J.H.; Pei, Y.Y.; Yuan, M.L.; Zhang, Y.L.; Dai, F.H.; Liu, Y.; Wang, Q.M.; Zheng, J.J.; Xu, L.; Holmes, E.C.; Zhang, Y.Z. A new coronavirus associated with human respiratory disease in china. *Nature* **2020**, *579*, 265-269.
2. Lauring, A.S.; Malani, P.N. Variants of SARS-CoV-2. *JAMA* **2021**.
3. Kannan, S.R.; Spratt, A.N.; Cohen, A.R.; Naqvi, S.H.; Chand, H.S.; Quinn, T.P.; Lorson, C.L.; Byrareddy, S.N.; Singh, K. Evolutionary analysis of the delta and delta plus variants of the SARS-CoV-2 viruses. *J Autoimmun* **2021**, *124*, 102715.
4. Harvey, W.T.; Carabelli, A.M.; Jackson, B.; Gupta, R.K.; Thomson, E.C.; Harrison, E.M.; Ludden, C.; Reeve, R.; Rambaut, A.; Peacock, S.J.; Robertson, D.L.; Consortium, C.-G.U. SARS-CoV-2 variants, spike mutations and immune escape. *Nature Reviews Microbiology* **2021**, *19*, 409-424.
5. Mittal, A.; Khattri, A.; Verma, V. Structural and antigenic variations in the spike protein of emerging SARS-CoV-2 variants. *PLoS Pathog* **2022**, *18*, e1010260.
6. Mahase, E. Covid-19: What do we know about omicron sublineages? *BMJ* **2022**, *376*, o358.
7. Schmidt, F. *Nature* **2021**.
8. Elbe, S.; Buckland-Merrett, G. Data, disease and diplomacy: Gisaid's innovative contribution to global health. *Glob Chall* **2017**, *1*, 33-46.
9. Hadfield, J.; Megill, C.; Bell, S.M.; Huddleston, J.; Potter, B.; Callender, C.; Sagulenko, P.; Bedford, T.; Neher, R.A. Nextstrain: Real-time tracking of pathogen evolution. *Bioinformatics* **2018**, *34*, 4121-4123.
10. Kannan, S.R.; Spratt, A.N.; Sharma, K.; Chand, H.S.; Byrareddy, S.N.; Singh, K. Omicron SARS-CoV-2 variant: Unique features and their impact on pre-existing antibodies. *J Autoimmun* **2022**, *126*, 102779.
11. Berman, H.M.; Westbrook, J.; Feng, Z.; Gilliland, G.; Bhat, T.N.; Weissig, H.; Shindyalov, I.N.; Bourne, P.E. The protein data bank. *Nucleic Acids Res* **2000**, *28*, 235-242.
12. McCallum, M.; Czudnochowski, N.; Rosen, L.E.; Zepeda, S.K.; Bowen, J.E.; Walls, A.C.; Hauser, K.; Joshi, A.; Stewart, C.; Dillen, J.R.; Powell, A.E.; Croll, T.I.; Nix, J.; Virgin, H.W.; Corti, D.; Snell, G.; Veesler, D. Structural basis of SARS-CoV-2 omicron immune evasion and receptor engagement. *Science* **2022**, *375*, 864-868.
13. Lan, J.; Ge, J.; Yu, J.; Shan, S.; Zhou, H.; Fan, S.; Zhang, Q.; Shi, X.; Wang, Q.; Zhang, L.; Wang, X. Structure of the SARS-CoV-2 spike receptor-binding domain bound to the ACE2 receptor. *Nature* **2020**, *581*, 215-220.
14. Mannar, D.; Saville, J.W.; Zhu, X.; Srivastava, S.S.; Berezuk, A.M.; Tuttle, K.S.; Marquez, A.C.; Sekirov, I.; Subramaniam, S. SARS-CoV-2 omicron variant: Antibody evasion and cryo-em structure of spike protein-ACE2 complex. *Science* **2022**, *375*, 760-764.
15. Cameroni, E.; Bowen, J.E.; Rosen, L.E.; Saliba, C.; Zepeda, S.K.; Culap, K.; Pinto, D.; VanBlargan, L.A.; De Marco, A.; di Iulio, J.; Zatta, F.; Kaiser, H.; Noack, J.; Farhat, N.; Czudnochowski, N.; Havenar-Daughton, C.; Sprouse, K.R.; Dillen, J.R.; Powell, A.E.; Chen, A.; Maher, C.; Yin, L.; Sun, D.; Soriaga, L.; Bassi, J.; Silacci-Fregni, C.; Gustafsson, C.; Franko, N.M.; Logue, J.; Iqbal, N.T.; Mazzitelli, I.; Geffner, J.; Grifantini, R.; Chu, H.; Gori, A.; Riva, A.; Giannini, O.; Ceschi, A.; Ferrari, P.; Cippà, P.E.; Franzetti-Pellanda, A.; Garzoni, C.; Halfmann, P.J.; Kawaoka, Y.; Hebner, C.; Purcell, L.A.; Piccoli, L.; Pizzuto, M.S.; Walls, A.C.; Diamond, M.S.; Telenti, A.; Virgin, H.W.; Lanzavecchia, A.; Snell, G.; Veesler, D.; Corti, D. Broadly neutralizing antibodies overcome SARS-CoV-2 omicron antigenic shift. *Nature* **2022**, *602*, 664-670.
16. Krissinel, E.; Henrick, K. Inference of macromolecular assemblies from crystalline state. *J Mol Biol* **2007**, *372*, 774-797.
17. Dong, J.; Zost, S.J.; Greaney, A.J.; Starr, T.N.; Dingens, A.S.; Chen, E.C.; Chen, R.E.; Case, J.B.; Sutton, R.E.; Gilchuk, P.; Rodriguez, J.; Armstrong, E.; Gainza, C.; Nargi, R.S.; Binshtein, E.; Xie, X.; Zhang, X.; Shi, P.Y.; Logue, J.; Weston, S.; McGrath, M.E.; Frieman, M.B.; Brady, T.; Tuffy, K.M.; Bright, H.; Loo, Y.M.; McTamney, P.M.; Esser, M.T.; Carnahan, R.H.; Diamond, M.S.; Bloom, J.D.; Crowe, J.E., Jr. Genetic and structural basis for SARS-CoV-2 variant neutralization by a two-antibody cocktail. *Nat Microbiol* **2021**, *6*, 1233-1244.

18. Zost, S.J.; Gilchuk, P.; Case, J.B.; Binshtein, E.; Chen, R.E.; Nkolola, J.P.; Schafer, A.; Reidy, J.X.; Trivette, A.; Nargi, R.S.; Sutton, R.E.; Suryadevara, N.; Martinez, D.R.; Williamson, L.E.; Chen, E.C.; Jones, T.; Day, S.; Myers, L.; Hassan, A.O.; Kafai, N.M.; Winkler, E.S.; Fox, J.M.; Shrihari, S.; Mueller, B.K.; Meiler, J.; Chandrashekar, A.; Mercado, N.B.; Steinhardt, J.J.; Ren, K.; Loo, Y.M.; Kallewaard, N.L.; McCune, B.T.; Keeler, S.P.; Holtzman, M.J.; Barouch, D.H.; Gralinski, L.E.; Baric, R.S.; Thackray, L.B.; Diamond, M.S.; Carnahan, R.H.; Crowe, J.E., Jr. Potently neutralizing and protective human antibodies against SARS-CoV-2. *Nature* **2020**, *584*, 443-449.
19. Saito, A.; Irie, T.; Suzuki, R.; Maemura, T.; Nasser, H.; Uriu, K.; Kosugi, Y.; Shirakawa, K.; Sadamasu, K.; Kimura, I.; Ito, J.; Wu, J.; Iwatsuki-Horimoto, K.; Ito, M.; Yamayoshi, S.; Loeber, S.; Tsuda, M.; Wang, L.; Ozono, S.; Butlertanaka, E.P.; Tanaka, Y.L.; Shimizu, R.; Shimizu, K.; Yoshimatsu, K.; Kawabata, R.; Sakaguchi, T.; Tokunaga, K.; Yoshida, I.; Asakura, H.; Nagashima, M.; Kazuma, Y.; Nomura, R.; Horisawa, Y.; Yoshimura, K.; Takaori-Kondo, A.; Imai, M.; Genotype to Phenotype Japan, C.; Tanaka, S.; Nakagawa, S.; Ikeda, T.; Fukuhara, T.; Kawaoka, Y.; Sato, K. Enhanced fusogenicity and pathogenicity of SARS-CoV-2 delta p681r mutation. *Nature* **2022**, *602*, 300-306.
20. Yan, L.; Yang, Y.; Li, M.; Zhang, Y.; Zheng, L.; Ge, J.; Huang, Y.C.; Liu, Z.; Wang, T.; Gao, S.; Zhang, R.; Huang, Y.Y.; Guddat, L.W.; Gao, Y.; Rao, Z.; Lou, Z. Coupling of n7-methyltransferase and 3'-5' exoribonuclease with SARS-CoV-2 polymerase reveals mechanisms for capping and proofreading. *Cell* **2021**, *184*, 3474-3485 e3411.
21. Zhao, Y.; Fang, C.; Zhang, Q.; Zhang, R.; Zhao, X.; Duan, Y.; Wang, H.; Zhu, Y.; Feng, L.; Zhao, J.; Shao, M.; Yang, X.; Zhang, L.; Peng, C.; Yang, K.; Ma, D.; Rao, Z.; Yang, H. Crystal structure of SARS-CoV-2 main protease in complex with protease inhibitor pf-07321332. *Protein Cell* **2021**.
22. Rockett, R.; Basile, K.; Maddocks, S.; Fong, W.; Agius, J.E.; Johnson-Mackinnon, J.; Arnott, A.; Chandra, S.; Gall, M.; Draper, J.; Martinez, E.; Sim, E.M.; Lee, C.; Ngo, C.; Ramsperger, M.; Ginn, A.N.; Wang, Q.; Fennell, M.; Ko, D.; Lim, H.L.; Gilroy, N.; O'Sullivan, M.V.N.; Chen, S.C.; Kok, J.; Dwyer, D.E.; Sintchenko, V. Resistance mutations in SARS-CoV-2 delta variant after sotrovimab use. *N Engl J Med* **2022**.
23. Katoh, K.; Standley, D.M. MAFFT multiple sequence alignment software version 7: Improvements in performance and usability. *Mol Biol Evol* **2013**, *30*, 772-780.
24. Kumar, S.; Stecher, G.; Li, M.; Knyaz, C.; Tamura, K. MEGA x: Molecular evolutionary genetics analysis across computing platforms. *Mol Biol Evol* **2018**, *35*, 1547-1549.
25. Troshin, P.V.; Procter, J.B.; Barton, G.J. Java bioinformatics analysis web services for multiple sequence alignment--jabaws:MSA. *Bioinformatics* **2011**, *27*, 2001-2002.
26. DeLano, W.L. An open-source molecular graphics tool. CCP4 newsletter on protein crystallography. **2002**, *40*, 82-92.
27. Jorgensen, W.L.; Chandrasekhar, J.; Madura, J.D.; Impey, R.W.; Klein, M.L. Comparison of simple potential functions for simulating liquid water. *Journal of Chemical Physics* **1983**, *79*, 926–935.
28. W Humphrey; A Dalke; Schulten, K. Vmd: Visual molecular dynamics. *Journal of Molecular Graphics* **1996**, *14*, 33-38.